On the treatment of electrostatic interactions of non-spherical molecules in equation of state models

Stephan Korden[a], Nguyen Van Nhu[a], Jadran Vrabec[b], Joachim Gross[c] and Kai Leonhard[ac]

[a]Lehrstuhl für Technische Thermodynamik
RWTH Aachen
52056 Aachen
Germany

[b]Thermodynamics and Energy Technology, University of Paderborn
Warburger Straße 100
33098 Paderborn
Germany

[c] Engineering Thermodynamics
Delft University of Technology
Leeghwaterstraat 44
2628 CA Delft
The Netherlands

email: leonhard@ltt.rwth-aachen.de
Phone: (+49)241-8098174
Fax: (+49)241-8092-255

March 26, 2010

Abstract

For predictive applications, equation of state (EOS) models have to describe all relevant physical interactions accurately. In this contribution, the vapor–liquid equilibria of various dipolar two-center Lennard-Jones model molecules are determined by molecular simulation, as function of molecular elongation and deflection angle of the dipole. It is shown that present PC-SAFT-based EOS models require additional adjustable parameters in order to describe the orientational effects of the dipole-moment. We present extensions of the model to avoid the additional parameters and apply the extended equations to model systems and real molecules.

Keywords:

SAFT; chemical thermodynamics; molecular properties; phase equilibria; perturbation theory; COSMO; continuum solvation model, prediction, vapor-liquid

1 Introduction

Equation of state (EOS) models are an established tool to describe thermodynamic properties of fluids and amorphous materials such as polymers [1].

While the well-known cubic EOSs are still applied in many industrial applications, models with a better physical basis have attracted much interest, in academia as well as in industry. The Statistical Associating Fluid Theory (SAFT) [2] is based on Wertheim's thermodynamic perturbation theory of first oder (TPT-1) [3, 4] and led to a group of successful equations of state. In this group of SAFT-type EOS models, TPT-1 is used to account for reversible association (e. g. hydrogen bonds) and irreversible bonding (chains formed by covalently bonded spheres). Main reasons for the success of the SAFT model are the good description of molecular size and flexibility effects, the explicit description of association interactions and the addition of dispersion and electrostatic terms in combination with a relatively simple form of the EOS. While the treatment of repulsion, chain formation and association is very similar in all SAFT models, there is some variation in the treatment of dispersion interactions and even more so concerning electrostatics. A comprehensive review of the development of SAFT-type models can be found in ref [1].

In the SAFT models, the residual Helmholtz energy A^{res} has several contributions, the hard sphere term, A^{hs}, the formation of chains, A^{chain}, the dispersion term, A^{disp}, one or more multipole–multipole contributions, A^{MM}, and an association contribution, A^{assoc}.

$$A^{\mathrm{res}} = A^{\mathrm{hs}} + A^{\mathrm{chain}} + A^{\mathrm{disp}} + A^{\mathrm{MM}} + A^{\mathrm{assoc}}. \tag{1}$$

Each non-polar component i is characterized by three pure component pa-

rameters: the number of m_i connected segments with a segment-diameter parameter σ_i and a dispersion energy parameter ϵ_i. This study is not concerned with associating compounds and we only mention that two pure component parameters and the definition of the number of associating sites are used to describe the associating interactions.

In many applications of SAFT models the multipolar contributions are accounted for only implicitly or not at all. Haslam et al. [5] have shown for the SAFT-VR model (where 'VR' is for a square-well potential of variable range) that an extension of the Hudson-McCoubrey combining rule leads to a predictive combination rule for electrostatic interactions in this model. The polar interactions are thereby treated as quasi-dispersive interactions. A temperature dependent and potentially large deviation of the binary square well depth from the geometric mean of those of the pure components can result from this procedure. However, this is not unphysical or a problem, as suggested by other authors (see refs. in [5]).

The polar contributions were in some studies explicitly formulated in terms of the Helmholtz energy. In most applications were these polar terms parameterized by adjusting effective dipole moments or quadrupolar moments (or related model-parameters) to experimental data [6, 7, 8, 9, 10, 11]. Since multipole interactions have a similar range as dispersion interactions, it is not unambiguous to determine meaningful pure component parameters. The flat minimum of the objective function for polar parameters and the strong correlation to the dispersion energy parameter has been noted by

Sauer et al. [7] and it is the basis for the work of Haslam et al. [5]. In recent approaches, these parameters are taken from experimental tabulations or from quantum mechanics [12, 13, 14, 15] so that no additional adjustable parameter is introduced with the multipolar terms.

In this contribution we consider the modeling of electrostatic interactions in the PC-SAFT model [16, 17] in more detail. In order to do so, we briefly review the present models for these interactions, and present molecular simulation results for model systems of two-center Lennard-Jones (2CLJ) potentials with multipoles rotated out of the symmetry axis of the molecular 2CLJ body, resulting in an effectively stronger interaction. Since these effects are not accounted for in the present models, we suggest extensions of the existing models and discuss the improvements achieved and the limitations that do still exist.

2 Equation of state modeling of electrostatic interactions

Sauer and Chapman [7] combined a model of Jog and Chapman [18, 6] where some of the segments carrry a dipole moment forming an angle of 90 degrees with the bond to the next segment with PC-SAFT and SAFT-HR. Here, the number polar segments appears as an additional parameter. The model has been applied sucessfully to, e.g., ketones [7]. An additional pure component parameter was thereby introduced, that was fitted to pure component data. Karakatsani et al. [10, 11] applied a perturbation theory with expressions for

correlation integrals of hard-spheres [19] together with the PC-SAFT EOS. An approach where the correlation integrals were set to constant values was also tested. An additional parameter for the spatial range of polar interactions was included [11]. There are several parameterizations for polar terms based on a hard-sphere reference [20, 19, 21]. Application of these terms to polar substances with SAFT-based EOS models (with an adjustable polar parameter) leads, according to our experience, in some cases to ambiguous results, where the best fit of the pure component behavior is obtained with the polar moment (or a related parameter) equal to zero.

New multipolar terms for quadrupole–quadrupole [12], dipole–dipole [13] and dipole–quadrupole [15] interactions were proposed in another approach, based on molecular simulations for the 2CLJ fluid. The resulting polar terms capture the effect of molecular elongation. However, the perturbation formalism has not been based on the pair correlation function of the non-spherical 2CLJ fluid, so that the polar moments are fixed point multipole moments oriented along the molecular axis. The advantage of this approach is that there is no structure of a reference fluid used explicitly which may spoil the results in the case of a strong perturbation. The disadvantage is that the approach is based on a molecular model where the dipole and quadrupole moments are always aligned with the symmetry axis of the molecules (see Fig. 1, right). The polar contributions were applied with the PC-SAFT EOS (then termed PCP-SAFT model). It was found that dipole and quadrupole values from experiment or quantum chemical calculations could be used for simple

molecules without introducing an additional adjustable parameter. The correlation results for pure components were also systematically improved, unlike to polar contributions earlier suggested, where an improvement of pure component behavior is found only in some cases. The treatment of more complex molecules with multiple polar sites, however, is so far not obvious.

Leonhard et al. have combined the perturbation theory (PT) with spherical reference [22, 23] with PC-SAFT, which they have termed PC-SAFTP1, for PC-SAFT polar, version 1 [14]. The pair correlation function (PCF) of the reference fluid, a one-center Lennard-Jones (1CLJ) fluid, has been determined by Monte Carlo (MC) simulations. In the same work [14] an empirical combination of PC-SAFT with the dipole–dipole term of PCP-SAFT and all other (dipole–quadrupole and quadrupole–quadrupole) terms from the PT with spherical reference was tested. The quadrupole terms have the advantage that the tensorial information of the multipolar moment is preserved. The disadvantage of the approach is that the accuracy of the perturbation series decreases when the PCF of the actual fluid is too different from the spherical reference PCF, i.e. when shape effects are too different from the spherical reference. Figure 1 visualizes the different approaches in the PCP-SAFT and the PC-SAFTP1 model.

The generalisation of perturbation theory with spherical reference to the non-spherical reference case may seem to be a logical next step. However, in addition to the complexity of the necessary mathematical expressions, Vega et al. [24] have shown that the PCF of the non-polar 2CLJ fluid changes

drastically when combined with a dipole moment deflected from the axis of symmetry of a strength typical for refrigerants. Therefore, this approach seems not very promising and we evaluated other approaches here: On the one hand the use of effective multipole moments, and on the other hand expressions that capture the angle of dipole moments towards the molecular elongation of small fluids.

Recently, we have shown that dipole moments, μ, and quadrupole moments, Θ, can be obtained from quantum mechanical calculations with high accuracy compared to experimental values [25, 26]. The average absolute deviation was found to be 2.6 % for the dipole moment and 4.2 % for the C_6 coefficient compared to experimental data. An accurate determination of the quadrupole moment is more difficult than for the dipole moment, experimentally as well as computationally. Not much accurate experimental data is available for a critical evaluation of our results.

EOS calculations have been performed with the ThermoC software package [27] and with software developed by us.

3 Molecular model

Two-center Lennard-Jones plus point dipole fluids (2CLJD) were investigated here by molecular simulation regarding their vapor-liquid phase behavior. The 2CLJD pair potential is composed of two identical Lennard-Jones sites separated by a fixed distance L (2CLJ) plus a point dipole with a moment μ placed in the geometric center of the molecule. In this work, the polarity

was not aligned along the molecular axis, but the dipole vector was inclined by an angle γ with respect to it, cf. Figure 2. The full potential writes as

$$\begin{aligned} u_{\mathrm{2CLJD}}(\boldsymbol{r}_{ij}, \boldsymbol{\omega}_i, \boldsymbol{\omega}_j, L, \mu, \gamma, \sigma, \epsilon) &= u_{\mathrm{2CLJ}}(\boldsymbol{r}_{ij}, \boldsymbol{\omega}_i, \boldsymbol{\omega}_j, L, \sigma, \epsilon) \\ &+ u_{\mathrm{D}}(\boldsymbol{r}_{ij}, \boldsymbol{\omega}_i, \boldsymbol{\omega}_j, \mu, \gamma), \end{aligned} \tag{2}$$

where

$$u_{\mathrm{2CLJ}}(\boldsymbol{r}_{ij}, \boldsymbol{\omega}_i, \boldsymbol{\omega}_j, L, \sigma, \epsilon) = \sum_{a=1}^{2} \sum_{b=1}^{2} 4\epsilon \left[\left(\frac{\sigma}{r_{ab}} \right)^{12} - \left(\frac{\sigma}{r_{ab}} \right)^{6} \right], \tag{3}$$

is the Lennard-Jones part. Herein, $\boldsymbol{r}_{ij}$ is the center-center distance vector of two molecules i and j, r_{ab} is one of the four Lennard-Jones site-site distances, a counts the two sites of molecule i, b counts those of molecule j. The vectors $\boldsymbol{\omega}_i$ and $\boldsymbol{\omega}_j$ represent the orientations of the two molecules. The Lennard-Jones parameters σ and ϵ represent size and energy, respectively. Two dipoles with the same moment μ interact with the potential

$$u_{\mathrm{D}}(\boldsymbol{r}_{ij}, \boldsymbol{\omega}_i, \boldsymbol{\omega}_j, \mu) = \frac{\mu^2}{|\boldsymbol{r}_{ij}|^3} \left(\sin\theta_i \sin\theta_j \cos\phi_{ij} - 2\cos\theta_i \cos\theta_j \right). \tag{4}$$

Note that θ_i is the angle between the dipole vector of molecule i and the connection line of the interacting dipoles, whereas ϕ_{ij} is the azimuthal angle between the dipole vectors of molecules i and j.

For very small intermolecular distances $|\boldsymbol{r}_{ij}|$ of more elongated fluids, the positive Lennard-Jones part u_{2CLJ} of the full potential cannot outweigh the divergence to $-\infty$ of the polar part u_{D}. This divergence of u_{2CLJD} leads to infinite Boltzmann factors, i.e. non-existence of the configurational integral. During molecular dynamics phase space sampling within the pressure

range in question, this artifact of the 2CLJD potential causes no problem as intermolecular dipole-dipole distances are very improbable to fall below critical values. However, during Monte-Carlo simulation or the calculation of entropic properties by test particle insertion [28], critical intermolecular dipole-dipole distances might occur. Following Möller and Fischer [29], a hard sphere of diameter 0.4σ was placed directly on the dipolar sites to prevent unphysically attractive interaction energies for critical configurations to avoid this problem.

The parameters σ and ϵ were used for the reduction of all thermodynamic properties as well as the other model parameters: $T^* = Tk_\mathrm{B}/\epsilon$, $p^* = p\sigma^3/\epsilon$, $\rho^* = \rho\sigma^3$, $h^* = h/\epsilon$, $L^* = L/\sigma$ and $\mu^{*2} = \mu^2/(\epsilon\sigma^3)$. For a specified reduced dipole moment $\mu^{*2} = 6$, elongation and inclination angle were varied in the following range: $L^* = 0.2$, 0.4, 0.6, 0.8 and 1 as well as $\gamma = 30$, 60 and 90°. In case of the elongation $L^* = 1$, where the Lennard-Jones part of the molecular model resembles two adjoining spheres, it was not feasible to simulate the inclination angles $\gamma = 60°$ and 90°. Thus, combining these values leads to a set of 13 model fluids that were investigated here, c.f. Table 1.

4 Molecular simulation method

For all VLE simulations, the Grand Equilibrium method [30] was used, where the temperature is the independent thermodynamic variable in case of a pure fluid.

In the first step, it samples the liquid phase in the isobaric-isothermal

ensemble at this temperature and some pressure not too far from the vapor pressure. Thereby, the chemical potential and its derivative with respect to the pressure, i.e. the molar volume, is determined. On the basis of these data, a first-order Taylor series for the pressure dependence of the chemical potential is known. In the second step, the Grand Equilibrium method samples the vapor phase by means of a pseudo grand canonical simulation. Here, the chemical potential is specified according to the Taylor series from the liquid, where the instantaneous pressure of the vapor phase is inserted. In this way, the vapor phase simulation is steered to the saturated state, where temperature, pressure and chemical potential of the two phases are equal.

In all simulations the center of mass cut-off radius was $r_\mathrm{c} = 5\sigma$. Outside the cut-off sphere, the fluid was assumed to have no preferential relative orientation of the molecules, i.e. for the calculation of the Lennard-Jones long range corrections, orientational averaging was done with equally weighted relative orientations as proposed by Lustig [31]. Long range corrections for the dipolar interaction were calculated with the reaction field method [32, 33], which has been demonstrated to yield reliable results for spherical and elongated dipolar molecules [34, 35]. the relative permittivity ϵ_s was set to infinity (tinfoil boundary condition).

Configuration space sampling was done with $N = 1372$ particles by molecular dynamics for liquid phase and $N = 500$ by Monte-Carlo for vapor phase simulations. For liquid phase simulations, the reduced integration time step

was set to $\Delta t\sqrt{m/\epsilon}/\sigma = 0.001$ and the reduced membrane mass parameter of Anderson's barostat [36] was set to $2 \cdot 10^{-5}$.

Starting from a face centered lattice arrangement, every liquid run was equilibrated over $100,000$ time steps. Data production was performed over $300,000$ time steps. At each production time step $4N$ test particles [28] were inserted into the liquid phase to calculate the chemical potential.

After an equilibration of 10,000 cycles, the vapor was sampled over 50,000 production cycles. One Monte Carlo loop is defined here as N trial translations, $(2/3)\,N$ trial rotations, one trial volume change as well as three insertion and deletion moves.

In some cases, where a highly dense and strongly polar liquid phase was present, the more elaborate gradual insertion scheme had to be employed to obtain the chemical potential with sufficient accuracy. The gradual insertion method is an expanded ensemble method [37] based on the Monte Carlo technique. Here, the version proposed by Nezbeda and Kolafa [38] was used, in a form that was extended to the NpT ensemble [39]. This concept leads to a considerably improved accuracy of the residual chemical potential. Gradual insertion simulations were performed with $N = 864$ particles in the liquid phase. Starting from a face-centered lattice arrangement, every simulation run was given $5,000$ Monte Carlo loops to equilibrate. Data production was performed over $100,000$ Monte Carlo loops. Further simulation parameters for runs with gradual insertion were taken from Vrabec et al. [39].

VLE data were determined for temperatures of about 55 % to 95 %

of T_c^*, which is dependent on L^*, μ^{*2} and γ. In the whole temperature range all thermodynamic properties of both phases were obtained by simulation. To conduct the large number of VLE calculations, a Grid-based Simulation Framework for Engineering Applications (GridSFEA) [40] was employed. This is an easy-to-use mechanism for application-independent parameter studies, which enables a checkpoint-based migration of long-running simulations in Grid environments.

5 Computation of effective reduced multipole moments based on a continuum solvation model

A first analysis of the results of the simulations has shown that the orientation of the multipole moments can have strong effects on thermodynamic properties which can be modeled by effective multipole moments, as described in the results section. It turned out that a continuum solvation model (CSM), namely the classical COnductor-like Screening Model (COSMO) [41], can be used to estimate the required effective multipole moments based on the ratio of the dielectric screening energy of the actual molecule to that of a spherical reference particle. In a CSM, a multipolar molecule is immersed in a fluid assumed to be a completely structureless but polarizable continuum with relative permittivity ϵ_r. Since the permittivity enters via a universal function into the screening energy (i.e. the function is independent from the shape of the molecule) in the COSMO model [41], it always cancels out in the re-

quired ratio. Therefore, the conversion from the real molecule to the effective spherical one is independent of the density and the composition of the environment of the solute molecule under consideration. We apply the COSMO model classically which means the computation of the dielectric energy for a given charge distribution, opposed to a quantum chemical calculation that is usually performed in combination with the COSMO model. The authors like to stress here that the COSMO model is different from the COMSO-RS model and, in contrast to the latter, well able to differentiate between dipolar and quadrupolar molecules. The probably more-widely known COSMO-RS model is an extention of the COSMO model. In COSMO-RS, intermolecular interactions are modeled on the basis of the surface charges obtained by the COSMO model and a statistical thermodynamical model of independent segments. By these statistics, the temperature, which is absent is the purely electrostatic COSMO model, is introduced into the COSMO-RS model.

For 2CLJ molecules a first approach consists of defining the COSMO cavity by replacing the LJ sites by spheres of diameter σ and keeping the bond length unchanged. COSMO cavities, however, should be space filling which is not the case for 2CLJ fluids at liquid densities. Therefore, the size of the COSMO cavities should be increased compared to the LJ segment diameter. Van der Waals radii increased by 15 to 20 % are usually employed in CSMs. Since we compare our results with a spherical cavity of the same volume, the absolute size of the radii is irrelevant. Instead, we rescale L^* by an adjustable, but system and state-independent, rescaling parameter

($L^*_{\mathrm{scaled}} = \alpha L^*_{\mathrm{COSMO}}$) to make the effective reduced dipole moments obtained via the COSMO model match those of the 2CLJ fluid.

We smooth the cusp between the two spheres to a radius r_{solvent} that is identical to the diameter of the segments [41]. Next, the dielectric screening energy is computed for the desired multipole moments and equated to the screening energy of the same multipole moments in a spherical cavity of radius r. Finally, we solve for r. The ratio of the sizes of both cavities determines the effective reduced multipole moment that has to be used in a perturbation theory with a spherical reference according to the CSM approach. Essentially, this procedure corresponds to the assumption that two different molecules having the same screening energy for any given relative permittivity ϵ_{r}, should also be described similarly by a perturbation theory.

For 2CLJ molecules, the reduced dipole and quadrupole moments are defined as

$$\mu^{*2}_{\mathrm{2CLJ}} = \frac{\mu^2}{\epsilon\sigma^3}, \tag{5}$$

$$Q^{*2}_{\mathrm{2CLJ}} = \frac{Q^2}{\epsilon\sigma^5}, \tag{6}$$

and in PC-SAFTP1 the reduced spherical (s) moments are defined as

$$\mu^{*2}_{\mathrm{s}} = \frac{\mu^2}{\epsilon V_{\mathrm{s}}}, \tag{7}$$

$$Q^{*2}_{\mathrm{s}} = \frac{Q^2}{\epsilon V_{\mathrm{s}}^{5/3}}. \tag{8}$$

Assuming identical energy parameters for the "real" and the effective spher-

ical molecule with volume $V_{\rm s}$, we obtain

$$\mu_{\rm s}^{*2} \;=\; \mu_{\rm 2CLJ}^{*2}\frac{\sigma^3}{V_{\rm s}}. \tag{9}$$

We note that for the 2CLJ model the volume of a site, not that of the molecule, has to be used. The effective reduced dipole moment with a spherical cavity is

$$\mu^{*}_{\rm eff,\ spherical} \;=\; \mu^{*}_{\rm 2CLJ}\sqrt{\frac{r^3_{\rm original\ site}}{V_{\rm s}}}, \tag{10}$$

where $V_{\rm s}$ is the volume of a spherical cavity with the same dielectric screening energy as the original cavity.

For real molecules, we compute the gas phase charge distribution on the MP2/aug-cc-pVDZ level and use the CHelp [42] method to fit atom-centered charges and point dipole moments to the electrostatic potential obtained from the full charge distribution using Gaussian09 [43]. These distributed multipole moments are then used in a COSMO calculation with standard COSMO radii. We feel that it makes more sense to use gas phase multipole moments than COSMO ones since the here-studied molecules have relatively low dielectric constants. A spherical particle is constructed with a point dipole and a point quadrupole moment in its center that reproduce the molecule's dipole and quadrupole moments and its volume is adjusted to obtain the same dielectric screening energy as for the real-shape particle. Finally, the effective reduced multipole moments for use in the PC-SAFTP1 model can

be obtained:

$$\mu^*_{\text{eff, spherical}} = \mu^*_{\text{QM}} \sqrt{\frac{V_{\text{COSMO, real molecule}}}{V_{\text{s}}}} \tag{11}$$

$$\Theta^*_{\text{eff, spherical}} = \Theta^*_{\text{QM}} \left(\frac{V_{\text{COSMO, real molecule}}}{V_{\text{s}}} \right)^{\frac{5}{6}} \tag{12}$$

$$\tag{13}$$

6 Results

6.1 Results and Discussion of the model systems

6.1.1 Comparison of equation of state theories to simulation results

Table 1 reports the VLE data of the regarded 13 model fluids. Vapor pressure p^*_σ, saturated liquid density ρ'^*, saturated vapor density ρ''^* and enthalpy of vaporization $\Delta h^{\text{v}\,*}$ are listed. The statistical uncertainties were determined by usual block averaging [44] and the error propagation law.

Figures 3 to 5 illustrate the strong influence of the deflection angle on the VLE data exemplarily for $L^* = 0.6$ and $\mu^{*2} = 6$. At constant elongation and dipole moment, the vapor-pressure curve decreases with growing deflection angle, corresponding to an increase of particle interaction (Figure 3). At the same time, the saturated liquid density (Figure 4) and the enthalpy of evaporation (Figure 5) increase with increasing deflection angle. Molecules are therefore closest packed at $\gamma = 90^o$, due to an effectively stronger polar interaction.

These results have a simple explanation, as illustrated in Figure 6: The

interaction of two dipoles, indicated by double cones and their overlapping regions, is hindered by the molecular geometry, i.e. by the two LJ sites in the present case. Although the dipolar potential is the same for all three cases, the average interaction energy is lowest (most negative) if the dipole is oriented perpendicular to the 2CLJ body axis. The results in Figures 3 to 5 show that the combination of the molecular shape and the orientation of its multipole moments have a strong effect on thermodynamic properties. The results also suggest to introduce effective reduced multipole moments to account for the fact that the accessible volume for favorable interactions depends on the deflection angle.

Two equation of state approaches are compared here to the molecular simulation data for the 2CLJD fluids. On the one hand, the dipole term of the original PCP-SAFT model combined with a 2CLJ equation of state (here abbreviated as 2CLJ-PCP). On the other hand, the dipole term of the original PC-SAFT-P1 model with a 2CLJ equation (abbreviated as 2CLJ-P1 model). The 2CLJ EOS proposed in [12] served as the equation of state for the non-polar 2CLJ fluid. Neither the2CLJ- P1 nor 2CLJ-PCP model take the effect of the deflection angle into account and it gets clear from Figures 3 to 5 that neither a spherical reference nor an elongated reference fluid with fixed dipole-angle are sufficient to describe these model fluids.

Solid lines in Figures 7 and 8 show the deviations in vapor pressure and saturated liquid density for the 2CLJ-P1 model with the molecular multipole moments for all elongations and deflection angels studied. The vapor pressure

of the 2CLJ-P1 model parameterized with an effective dipole moment is sometimes only half of that of the molecular simulation, while the 2CLJ-PCP model can produce results almost twice as large as the correct ones. Liquid densities deviate by 5 to 10 % for the 2CLJ-P1 model.

6.1.2 Individually adjusted effective dipole moments

When an effective multipole moment is fitted to each model system, the vapor pressure deviations can be reduced to 2–6 % for almost all systems (data not included in Figure 7). These results show that adjusted effective multipolar moments can be used to model deflected multipole moments, but all predictivity is lost if they have to be adjusted to data. Effectively, this approach requires the introduction of at least one additional adjustable parameter for real molecules, similar to other approaches [7, 11].

6.1.3 Angle dependent expansion coefficients

An alternative approach is to extend the parameterization of the polar PCP-terms to account for the deflection angle. Five parameters were adjusted to the molecular simulation data of Table 1. In the nomenclature of ref. [13],

we get the parameters

$$\begin{aligned} a_{10} &= \hat{a}_{10} + 0.20144 \cdot \sin^2\gamma \\ a_{20} &= \hat{a}_{20} - 1.7411 \cdot \sin^2\gamma \\ a_{11} &= \hat{a}_{11} + 1.3165 \cdot \sin^2\gamma \\ c_{10} &= \hat{c}_{10} + 0.28503 \cdot \sin^2\gamma \\ c_{20} &= \hat{c}_{20} + 2.2195 \cdot \sin^2\gamma \end{aligned} \tag{14}$$

where the coefficients indicated by the hat are the ones published earlier for 2CLJD fluids with axially aligned dipole moments [13]. The resulting EOS is in good agreement to molecular simulation data, as Figures 9 and 10 show. When these terms are applied to butanone or pentanone, however, and the angle is optimized one gets the angle zero to be most optimal. We suspect, that the 2CLJ fluid with multipole moment located between the two sites is not the most suitable reference for real fluids. In addition, the strategy can not be extended to molecules with multiple polar sites.

6.1.4 Continuum solvent modeling

For predictive applications, a model without additional adjustable parameters, however, is highly desirable, even if some accuracy has to be sacrificed. Figure 11 shows a comparison of reduced multipole moments fitted to VLE data obtained by molecular simulation and those determined directly by the COSMO model, as described in section 5. For all systems, COSMO cavities were chosen to be a factor of 1.7 larger than the LJ diameter σ. The

CSM-based results show a quite similar behavior, even though all structure except that of the central molecule is neglected. The individually fitted dipole moment for $L^* = 0$ is almost 3 % smaller than the CSM-based one (which is identical to the original one) because the Padé approximation in the perturbation theory overestimates the effects of strong multipoles, even for spherical particles.

When the CSM-based effective reduced dipole moments are used in the 2CLJ-P1 EOS model, the dashed lines in Figures 7 and 8 are obtained. For most systems, the vapor pressure deviations can be reduced to 3 to 8 % with this predictive model. Exceptions are an elongation of 1.0 with a deflection angle of 30 and $L^* = 0.8$ with $\gamma = 60^o$ at low temperature. For these elongations, the 2CLJ molecules are somewhat artificial since the multipole moments in real molecules cannot approach as closely as in the model molecules because of repulsive interactions. For the liquid volume, however, on average no improvement is found by using effective multipole moments.

The CSM-based approach opens up the opportunity to predictively compute effective multipole moments not only for 2CLJD molecules, but the basic assumptions should also allow to model more complicated molecules by a perturbation theory with a spherical reference. This is especially interesting when no axis of "near" rotational-symmetry axis exists. For the future, improvement should be possible by including one (or more) solvation shell(s) into the CSM model.

6.2 Application of the CSM formalism to real molecules

For some molecules, for which an unsatisfactory performance of the PC-SAFTP1 model was known and/or could be expected from the molecule's charge distribution, we compared the performance of the model with quantum chemically obtained gas phase multipole moments and effective ones. Interesting are linear molecules, e.g. acetonitrile ($NCCH_3$), and molecules that deviate strongly from rotational symmetry, (e.g. butanone). In addition to the effects studied with the model molecules in the previous section, both molecules have off-center multipole moments. Molecules that have a strong hexadecapole moment, (e.g. CO and C_2H_2) are also interesting, since the hexadecapole moment is not accounted for in our present EOS models, but Wojcik and Gubbins [45] found that it can have a strong decreasing effect on the effective quadrupole moment. It was also observed by us that the PC-SAFTP1 and the PCP-SAFT models show more accurate results for such molecules when quadrupole moments smaller than the best available experimental or theoretical values are used.

Table 2 shows the calculated gas phase multipole moments and the three adjusted PC-SAFTP1 parameters ϵ, σ, and m as well as the same data for effective multipole moments computed as described in section 5. The effective multipole moments predicted with the COSMO model on average allow for a more accurate correlation of experimental VLE data with the usual three adjustable parameters than the original gas phase moments do, see Table 3. We note that the effective multipole moments for nitrogen, ethyne,

and carbon monoxide are smaller than the gas phase ones. This coincides with our expectations because of the zero degree orientation and because of the hexadecapole moment with should also decrease the effective quadrupole moment. For butanone, the effective multipole moments are larger than the original ones. This is mainly because of the 90 degree deflection of the carbonyl group and its off-center position. The effective moments increase for acetonitrile, too, even though its dipole moment has a zero degree orientation. This is probably due to its vicinity of the cavity boundary in the COSMO calculation leading to a pronounced interaction with the continuum. In real acetonitrile, no dipole moment of a second molecule can come in such a favorable position. Therefore, the continuum approach may be insufficient for strongly asymmetric molecules and one solvation shell of explicit molecules may be necessary in the CSM calculation. This will be the objective of a future investigation.

7 Conclusion

We have shown by molecular simulation that the orientation of molecular multipole moments with respect to the molecular shape has a strong influence on the fluid's thermodynamic properties. We found that even a simple PT with spherical reference can reproduce the simulation data reasonably when effective multipole moments are used. These effective moments can be estimated via the dielectric screening energy obtained from a continuum solvation model for the model molecules and not too asymmetric real molecules.

The approach can also be applied to molecules with multiple polar sites. Further investigation of this approach will probably lead to EOS models with a better predictivity.

8 Acknowledgments

We gratefully acknowledge financial support from the German research council (Deutsche Forschungs Gemeinschaft, DFG) within the priority programme SPP 1155 by grant LE2221/2 and through the cluster of excellence "Tailor-made Fuels From Biomass" (EXC236) as well as from the GRANT program of the Delft University of Technology.

List of Symbols and Abbreviations

Latin alphabet

COSMO	Conductor like Screening MOdel
CSM	Continuum Solvation Model
d	effective segment diameter
EOS	Equation Of State
h	enthalpy
A	free energy
a	interaction site index
b	interaction site index
h	enthalpy
i	molecule index
j	molecule index
k_{B}	Boltzmann constant
L	molecular elongation
m	number of segments
MC	Monte Carlo
N	number of particles
p	pressure
PCF	Pair Correlation Function
PC-SAFT	Perturbed-Chain Statistical Associating Fluid Theory
PCP-SAFT	Perturbed-Chain Polar Statistical Associating Fluid Theory
PC-SAFTP1	Perturbed-Chain Statistical Associating Fluid Theory Polar
PT	Perturbation Theory
r	site-site distance
r_{c}	center of mass cut-off radius
SAFT	Statistical Associating Fluid Theory
SAFT-HR	Statistical Associating Fluid Theory by Huang and Radosz
SAFT-VR	Statistical Associating Fluid Theory with attraction of Variable Range
T	temperature
TPT	Thermodynamic Perturbation Theory
u	pair potential

Vector properties

$\boldsymbol{r}$	position vector
$\boldsymbol{\omega}$	orientation vector

Greek alphabet

γ	inclination angle
Δh^{v}	enthalpy of vaporization
Δt	integration time step
ϵ	Lennard-Jones energy parameter (in simulations)
	square-well depth parameter (in EOS)
ϵ_{s}	relative permittivity of dielectric continuum
θ_i	angle of nutation of molecule i
μ	dipolar moment
ρ	density
σ	Lennard-Jones size parameter
ϕ_{ij}	azimuthal angle between the dipole vectors of molecules i and j

Subscript

D	dipole
i	molecule index
j	molecule index
1CLJ	one-center Lennard-Jones
2CLJ	two-center Lennard-Jones
2CLJD	two-center Lennard-Jones plus point dipole

Superscript

*	reduced property
′	saturated liquid
″	saturated vapor
assoc	association
chain	chain
disp	dispersion
hs	hard sphere
MM	multipole–multipole
res	residual

References

[1] Sugata P. Tan, Hertanto Adidharma, and Maciej Radosz. Recent advances and applications of statistical associating fluid theory. *Ind. Eng. Chem. Res.*, 47:8063–8082, 2008.

[2] Walter G. Chapman, Keith E. Gubbins, George Jackson, and Maciej Radosz. Saft: Equation-of-state solution model for associating fluids. *Fluid Phase Equilib.*, 52:31–38, 1989.

[3] M. S. Wertheim. Fluids with highly directional attractive forces. I. Statistical thermodynamics. *J. Stat. Phys.*, 35:19–34, 1984.

[4] M. S. Wertheim. Fluids with highly directional attractive forces. II. Thermodynamic perturbation theory and integral equations. *J. Stat. Phys.*, 35:35–47, 1984.

[5] Andrew J. Haslam, Amparo Galindo, and George Jackson. Prediction of binary intermolecular potential parameters for use in modelling fluid mixtures. *Fluid Physe Equilib.*, 266:105–128, 2008.

[6] Prasanna K. Jog, Sharon G. Sauer, Jorg Blaesing, and Walter G. Chapman. Application of dipolar chain theory to the physe behavior of polar fluids and mixtures. *Ind. Eng. Chem. Rss.*, 40:4641–4648, 2001.

[7] S. G. Sauer and W. G. Chapman. A parametric study of dipolar chain theory with applications to ketone mixtures. *Ind. Eng. Chem. Res.*, 42:5687–5696, 2003.

[8] J. Gross and G. Sadowski. Perturbed-chain saft: Development of a new equation of state for simple, associating, multipolar and polymeric compounds. *In: Brunner G, ed. Supercritical fluids as solvents and reaction media. Amsterdam, the Netherlands: Elsevier Science*, pages 295–322, 2004.

[9] F. Tumakaka and G. Sadowski. Application of the perturbed-chain saft equation of state to polar systems. *Fluid Phase Equilib.*, 217:233–239, 2004.

[10] EK Karakatsani, T Spyriouni, and IG Economou. Extended statistical associating fluid theory (SAFT) equations of state for dipolar fluids. *AIChE J.*, 51:2328–2342, 2005.

[11] Eirini K. Karakatsani and Ioannis G. Economou. Perturbed chain-statistical associating fluid theory extended to dipolar and quadrupolar molecular fluids. *J. Phys. Chem. B*, 110:9252–9261, 2006.

[12] Joachim Gross. An equation of state contribution for polar components: Quadrupolar molecules. *AIChE J.*, 51:2556–2568, 2005.

[13] Joachim Gross and Jadran Vrabec. An equation of state contribution for polar components: Dipolar molecules. *AIChE J.*, 52:1194–1201, 2006.

[14] Kai Leonhard, Nguyen Van Nhu, and Klaus Lucas. Predictive equation of state models with parameters determined from quantum chemistry. Part 3: Improved treatment of multipolar interactions in a PC-SAFT based equation of state. *J. Phys. Chem. C*, 111:15533–15543, 2007.

[15] J. Vrabec and J. Gross. A molecular based approach to dipolar and quadrupolar fluids: Vapor-liquid equilibria simulation and an equation of state contribution for dipole-quadrupole interactions. *J. Phys. Chem. B*, 112:51–60, 2008.

[16] J Gross and G Sadowski. Application of perturbation theory to a hard-chain reference fluid: an equation of state for square-well chains. *Fluid Phase Equilib.*, 168:183–199, 2000.

[17] J. Gross and G. Sadowski. Perturbed-chain saft: An equation of state based on a perturbation theory for chain molecules. *Ind. Eng. Chem. Res.*, 40(4):1244–1260, 2001.

[18] Prasanna K. Jog and Walter G. Chapman. Application of Wertheim's thermodynamic perturbation theory to dipolar hard sphere chains. *Mol. Phys.*, 97:307–319, 1999.

[19] B. Larsen, J. C. Rasaiah, and G. Stell. Thermodynmic Perturbation-Theory for Multipolar and Ionic Liquids. *Mol. Phys.*, 33(4):987–1027, 1977.

[20] G. S. Rushbrooke, G. Stell, and J.S. Hye. Theory of polar liquids. i. dipolar hard spheres. *Mol. Phys.*, 26:1199–1215, 1973.

[21] D. Henderson, L. Blum, and A. Tani. Equation of state of ionic fluids. *ACS Symp. Ser.*, 300:281–296, 1986.

[22] C. G. Gray and K. E. Gubbins. *Theory of Molecular Fluids.* Clarendon press, 1984.

[23] Klaus Lucas. *Molecular Models for Fluids.* Cambridge University Press, 2007.

[24] Carlos Vega, Berthold Saager, and Johann Fischer. Molecular dynamics studies for the new refrigerant R152a with simple model potentials. *Mol. Phys.*, 68:1079–1093, 1989.

[25] Mahendra Singh, Kai Leonhard, and Klaus Lucas. Predictive equation of state models with parameters determined from quantum chemistry. Part 1: Determination of molecular properties. *Fluid Phase Equilib.*, 258:16–28, 2007.

[26] Kai Leonhard, Nguyen Van Nhu, and Klaus Lucas. Predictive equation of state models with parameters determined from quantum chemistry. Part 2: Improvement of the predictive performance of the PCP-SAFT equation of state. *Fluid Phase Equilib.*, 258:41–50, 2007.

[27] Ulrich K. Deiters. A modular program system for the calculation of thermodynamic properties of fluids. *Chem. Eng. Technol.*, 23:581–584, 2000.

[28] B. Widom. Some topics in the theory of fluids. *J. Chem. Phys.*, 39:2808–2812, 1963.

[29] D. Möller and J. Fischer. Determination of an effective intermolecular potential for carbon-dioxide using vapor liquid-phase equilibria from npt plus test particle simulations. *Fluid Physe Equilib.*, 100:35–61, 1994.

[30] J. Vrabec and H. Hasse. Grand equilibrium: Vapour-liquid equilibria by a new molecular simulation method. *Mol. Phys.*, 100:3375–3383, 2002.

[31] R. Lustig. Angle-average for the powers of the distance between 2 separated vectors. *Mol. Phys.*, 65:175–179, 1988.

[32] J. A. Barker and R. O. Watts. Monte Carlo studies of the dielectric properties of water-like models. *Mol. Phys.*, 26:789–792, 1973.

[33] B. Saager, J. Fischer, and M. Neumann. Reaction field simulations of monatomic and diatomic dipolar fluids. *Mol. Sim.*, 6:27–49, 1991.

[34] Alejandro Gil-Villegas, Simon C. Mc Grother, and George Jackson. Reaction-field and Ewald summation methods in Monte Carlo simulations of dipolar liquid crystals. *Mol. Phys.*, 92:723–734, 1997.

[35] Carlos Avendano and Alejandro Gil-Villegas. Monte Carlo simulations of primitive models for ionic systems using the Wolf method. *Mol. Phys.*, 104:1475–1486, 2006.

[36] H. C. Andersen. Molecular-dynamics simulations at constant pressure and-or temperature. *J. Chem. Phys.*, 72:2384–2393, 1980.

[37] S. V. Shevkunov, A. A. Martinovski, and P. N. Vorontsov-Velyaminov. *igh Temp. Phys. (USSR)*, 26:246, 1988.

[38] I. Nezbeda and J. Kolafa. New version of the insertion particle method for determining the chemical potential by Monte Carlo simulations. *Mol. Sim.*, 5:391–403, 1991.

[39] J. Vrabec, M. Kettler, and H. Hasse. Chemical potential of quadrupolar two-centre Lennard-Jones fluids by gradual insertion. *Chem. Phys. Lett.*, 356:431–436, 2002.

[40] I. L. Muntean, E. Elts, Buchholz M., and H.-J. Bungartz. Grid-supported simulation of vapour-liquid equilibria with GridSFEA. Lecture Notes in Computer Science 5101:45–55, 2008.

[41] A. Klamt and G. Schüürmann. COSMO: A new approach to dielectric screening in solvents with explicit expressions for the screening energy and its gradient. *J. Chem. Soc. Perkin Trans. II*, pages 799–805, 1993.

[42] L. E. Chirlian and M. M. Francl. Atomic charges derived from electrostatic potentials — a detailed study. *J. Comp. Chem.*, 8:894–905, 1987.

[43] M. J. Frisch et. al. Gaussian 09, 2009.

[44] H. Flyvbjerg and H. G. Petersen. Error estimates on averages of correlated data. *J. Chem. Phys.*, 91:461–466, 1989.

[45] M. C. Wojcik and K.E. Gubbins. Pure quadrupolar dumbbell fluids. theory and simulation. *J. Phys. Chem.*, 88:6559–6566, 1984.

9 Tables

Table 1: Vapor-liquid equilibrium data of different 2CLJD model fluids with $\mu^{*2} = 6$. For the low temperature state points indicated by †, the data are based on the chemical potential calculated by gradual insertion in the liquid. Otherwise, Widom's insertion method was used. The number in parentheses indicates the statistical uncertainty in the last decimal digit.

T^*	p^*_σ	ρ'^*	ρ''^*	$\Delta h^{\mathrm{v}\,*}$
$L^* = 0.2$, $\gamma = 30°$				
2.88	0.0058 (3)	0.7428 (2)	0.0021 (1)	28.9 (1)
3.14	0.0132 (5)	0.7138 (2)	0.0044 (2)	27.7 (1)
3.4	0.0270 (4)	0.6839 (2)	0.0087 (1)	26.2 (1)
3.66	0.0490 (5)	0.6521 (3)	0.0153 (2)	24.6 (1)
3.93	0.0838 (6)	0.6157 (4)	0.0259 (2)	22.6 (1)
4.19	0.1295 (7)	0.5753 (5)	0.0404 (2)	20.2 (1)
4.45	0.198 (1)	0.5301 (7)	0.0654 (4)	17.2 (1)
4.71	0.277 (1)	0.468 (2)	0.0982 (5)	13.6 (1)
4.97	0.381 (2)	0.387 (4)	0.1587 (8)	8.2 (2)
$L^* = 0.4$, $\gamma = 30°$				
1.97	0.0013 (1)	0.6215 (1)	0.00065 (6)	23.1 (1)
2.15	0.0032 (2)	0.6001 (1)	0.0015 (1)	22.2 (1)
2.33	0.0073 (2)	0.5787 (2)	0.00330 (9)	21.3 (1)
2.51	0.0144 (3)	0.5555 (2)	0.0062 (1)	20.2 (1)
2.69	0.0250 (3)	0.5306 (3)	0.0105 (1)	19.0 (1)
2.87	0.0421 (3)	0.5039 (3)	0.0175 (1)	17.7 (1)
3.05	0.0664 (5)	0.4746 (4)	0.0279 (2)	16.0 (1)
3.23	0.1001 (6)	0.4412 (4)	0.0437 (2)	13.9 (1)
3.41	0.142 (1)	0.396 (1)	0.0667 (5)	11.4 (1)
$L^* = 0.6$, $\gamma = 30°$				
1.54 †	0.00064 (3)	0.5253 (3)	0.00042 (2)	19.2 (1)
1.7	0.0020 (1)	0.5045 (1)	0.00122 (7)	18.4 (1)
1.84	0.0044 (2)	0.4860 (1)	0.0026 (1)	17.5 (1)
1.98	0.0090 (2)	0.4664 (2)	0.0049 (1)	16.6 (1)
2.12	0.0151 (3)	0.4450 (2)	0.0080 (2)	15.7 (1)
2.27	0.0273 (3)	0.4203 (2)	0.0145 (1)	14.4 (1)
2.41	0.0444 (3)	0.3946 (3)	0.0241 (2)	12.8 (1)
2.55	0.0663 (4)	0.3649 (6)	0.0376 (3)	11.1 (1)
2.69	0.0946 (5)	0.3266 (8)	0.0584 (3)	8.9 (1)

Table 1: continued.

T^*	p^*_σ	ρ'^*	ρ''^*	$\Delta h^{v\,*}$
$L^* = 0.8$, $\gamma = 30°$				
1.27 †	0.00022 (1)	0.4710 (3)	0.00017 (1)	17.7 (1)
1.28	0.00032 (8)	0.4692 (1)	0.00026 (6)	17.7 (1)
1.4	0.0010 (1)	0.4527 (1)	0.0007 (1)	16.9 (1)
1.51	0.0020 (2)	0.4365 (1)	0.0014 (2)	16.2 (1)
1.63	0.0043 (2)	0.4182 (1)	0.0028 (1)	15.3 (1)
1.75	0.0085 (3)	0.3992 (2)	0.0054 (2)	14.3 (1)
1.86	0.0145 (3)	0.3801 (2)	0.0091 (2)	13.3 (1)
1.98	0.0249 (2)	0.3570 (3)	0.0158 (2)	12.0 (1)
2.1	0.0397 (3)	0.3309 (4)	0.0263 (2)	10.6 (1)
2.21	0.0573 (3)	0.3008 (4)	0.0402 (2)	8.8 (1)
$L^* = 1$, $\gamma = 30°$				
1.17 †	0.00012 (1)	0.4466 (3)	0.00010 (1)	18.6 (1)
1.2	0.00023 (9)	0.4412 (1)	0.00020 (8)	18.3 (1)
1.31	0.0005 (1)	0.4220 (1)	0.00038 (9)	17.3 (1)
1.42	0.0016 (5)	0.4029 (1)	0.0011 (4)	16.1 (1)
1.53	0.0040 (4)	0.3826 (1)	0.0028 (3)	14.9 (1)
1.64	0.0077 (6)	0.3619 (2)	0.0053 (4)	13.8 (1)
1.75	0.0159 (4)	0.3396 (3)	0.0111 (3)	12.3 (1)
1.85	0.0258 (3)	0.3164 (3)	0.0186 (2)	10.9 (1)
1.96	0.0390 (5)	0.2857 (6)	0.0291 (4)	9.2 (1)
2.07	0.0611 (4)	0.246 (1)	0.0535 (3)	6.6 (1)
$L^* = 0.2$, $\gamma = 60°$				
2.82	0.0039 (3)	0.7548 (2)	0.0014 (1)	30.1 (1)
3.08	0.0096 (3)	0.7261 (2)	0.0032 (4)	28.8 (1)
3.34	0.0206 (4)	0.6978 (2)	0.0066 (1)	27.3 (1)
3.59	0.0377 (4)	0.6682 (3)	0.0117 (1)	25.9 (1)
3.85	0.0656 (6)	0.6348 (4)	0.0200 (2)	24.1 (1)
4.11	0.1038 (6)	0.5968 (5)	0.0315 (2)	22.0 (1)
4.36	0.1567 (8)	0.5578 (5)	0.0488 (3)	19.5 (1)
4.62	0.235 (1)	0.5083 (9)	0.0790 (4)	16.1 (1)
4.88	0.332 (2)	0.434 (3)	0.1307 (7)	11.0 (1)

Table 1: continued.

T^*	p^*_σ	ρ'^*	ρ''^*	$\Delta h^{v\,*}$
$L^* = 0.4$, $\gamma = 60°$				
2.09	0.0012 (2)	0.6210 (1)	0.0006 (1)	24.5 (1)
2.28	0.0032 (4)	0.5989 (2)	0.0014 (2)	23.5 (1)
2.47	0.0089 (3)	0.5762 (2)	0.0038 (1)	22.4 (1)
2.67	0.0174 (4)	0.5502 (2)	0.0071 (2)	21.1 (1)
2.7	0.0190 (2)	0.5454 (4)	0.0078 (1)	20.8 (1)
2.8	0.0256 (3)	0.5317 (4)	0.0103 (1)	20.1 (1)
2.86	0.0314 (4)	0.5242 (3)	0.0127 (1)	19.7 (1)
2.9	0.0351 (5)	0.5196 (5)	0.0141 (2)	19.4 (1)
3.0	0.0453 (6)	0.5034 (6)	0.0182 (2)	18.5 (1)
3.05	0.0522 (5)	0.4953 (4)	0.0210 (2)	18.0 (1)
3.24	0.0807 (6)	0.4615 (4)	0.0331 (2)	16.0 (1)
3.43	0.1201 (6)	0.4225 (7)	0.0518 (2)	13.6 (1)
3.62	0.173 (1)	0.370 (4)	0.0838 (5)	10.2 (1)
$L^* = 0.6$, $\gamma = 60°$				
1.54	0.00007 (6)	0.5458 (1)	0.00005 (4)	22.7 (1)
1.68	0.0002 (2)	0.5287 (1)	0.00012 (1)	21.8 (1)
1.82	0.0019 (2)	0.5110 (1)	0.0011 (1)	20.7 (1)
1.96	0.0043 (4)	0.4929 (1)	0.0023 (2)	19.8 (1)
2.1	0.0078 (3)	0.4734 (2)	0.0040 (1)	18.8 (1)
2.24	0.0146 (3)	0.4531 (2)	0.0074 (1)	17.6 (1)
2.38	0.0247 (4)	0.4316 (2)	0.0123 (2)	16.4 (1)
2.5	0.0360 (4)	0.4114 (5)	0.0180 (2)	15.2 (1)
2.52	0.0395 (3)	0.4065 (4)	0.0200 (2)	14.9 (1)
2.6	0.0473 (5)	0.3903 (7)	0.0237 (2)	14.0 (1)
2.66	0.0587 (4)	0.3785 (8)	0.0304 (2)	13.2 (1)
2.7	0.0624 (7)	0.3682 (9)	0.0319 (3)	12.7 (1)
2.8	0.0851 (6)	0.3426 (9)	0.0472 (3)	10.9 (1)
$L^* = 0.8$, $\gamma = 60°$				
1.43 †	0.00017 (1)	0.4881 (3)	0.00012 (1)	23.5 (1)
1.54	0.0012 (3)	0.4718 (1)	0.0008 (2)	22.1 (1)
1.68	0.0014 (5)	0.4510 (1)	0.0009 (3)	20.8 (1)
1.82	0.0055 (4)	0.4300 (1)	0.0033 (3)	19.0 (1)
1.96	0.0093 (6)	0.4074 (2)	0.0054 (4)	17.6 (1)
2.1	0.018 (1)	0.3826 (2)	0.0100 (6)	16.0 (1)
2.24	0.0310 (7)	0.3553 (7)	0.0179 (4)	14.0 (1)
2.38	0.0503 (7)	0.322 (2)	0.0305 (4)	11.6 (1)
2.52	0.0794 (8)	0.284 (4)	0.0549 (5)	8.7 (1)
2.66	0.115 (1)	0.244 (8)	0.0955 (9)	5.3 (1)

Table 1: continued.

T^*	p^*_σ	ρ'^*	ρ''^*	$\Delta h^{v\,*}$
$L^* = 0.2$, $\gamma = 90°$				
2.86	0.0038 (2)	0.7535 (2)	0.00137 (8)	30.4 (1)
3.12	0.0104 (4)	0.7250 (2)	0.0035 (1)	29.0 (1)
3.38	0.0223 (4)	0.6962 (2)	0.0071 (1)	27.6 (1)
3.64	0.0394 (4)	0.6654 (3)	0.0121 (1)	26.0 (1)
3.9	0.0684 (7)	0.6319 (4)	0.0207 (2)	24.2 (1)
4.16	0.1089 (7)	0.5943 (5)	0.0330 (2)	22.0 (1)
4.42	0.1672 (9)	0.5510 (7)	0.0524 (3)	19.3 (1)
4.68	0.242 (1)	0.499 (2)	0.0816 (5)	15.7 (1)
$L^* = 0.4$, $\gamma = 90°$				
2.15	0.0014 (3)	0.6213 (1)	0.0007 (2)	25.3 (1)
2.34	0.0043 (3)	0.5996 (2)	0.0019 (1)	24.3 (1)
2.54	0.0091 (4)	0.5748 (2)	0.0038 (2)	23.0 (1)
2.73	0.0169 (8)	0.5506 (2)	0.0068 (3)	21.7 (1)
2.93	0.0327 (3)	0.5233 (3)	0.0129 (1)	20.2 (1)
3.12	0.0549 (4)	0.4946 (3)	0.0218 (2)	18.5 (1)
3.31	0.0832 (5)	0.4617 (5)	0.0335 (2)	16.5 (1)
3.51	0.1274 (9)	0.420 (1)	0.0553 (4)	13.7 (1)
3.7	0.178 (1)	0.363 (5)	0.0850 (1)	10.2 (1)
$L^* = 0.6$, $\gamma = 90°$				
1.70 †	0.00044 (3)	0.5389 (4)	0.00026 (2)	23.9 (1)
1.76	0.0009 (1)	0.5304 (1)	0.00054 (8)	23.4 (1)
1.92	0.0027 (2)	0.5103 (1)	0.0015 (1)	22.1 (1)
2.08	0.0055 (4)	0.4898 (2)	0.0028 (2)	20.9 (1)
2.24	0.0110 (4)	0.4676 (2)	0.0055 (2)	19.6 (1)
2.40	0.0194 (4)	0.4432 (2)	0.0093 (2)	18.1 (1)
2.56	0.0332 (5)	0.4165 (4)	0.0159 (2)	16.4 (1)
2.72	0.0546 (6)	0.3868 (9)	0.0270 (3)	14.4 (1)
2.88	0.0848 (7)	0.351 (2)	0.0454 (4)	11.8 (1)
3.04	0.1260 (7)	0.313 (5)	0.0787 (4)	8.5 (1)

Table 1: continued.

$L^* = 0.8$, $\gamma = 90^\circ$				
1.56	0.0012 (8)	0.4985 (2)	0.0009 (6)	27.9 (1)
1.69	0.0031 (8)	0.4795 (2)	0.0022 (6)	25.4 (1)
1.95	0.0067 (7)	0.4394 (2)	0.0039 (4)	22.7 (1)
2.08	0.009 (1)	0.4175 (2)	0.0049 (7)	21.0 (1)
2.21	0.015 (1)	0.3938 (2)	0.0080 (5)	19.1 (1)
2.34	0.0302 (9)	0.3691 (3)	0.0169 (5)	16.5 (1)
2.47	0.043 (1)	0.3387 (5)	0.0233 (6)	14.5 (1)
2.6	0.0685 (8)	0.3047 (8)	0.0423 (5)	11.5 (1)

Table 2: Gas phase MP2/aug-cc-pVDZ//B3LYP/TZVP dipole and quadrupole moments, effective multipole moments and PC-SAFTP1 parameters.

	N_2	CO	C_2H_2	acetonitrile	butanone
with gas phase multipole moments:					
μ_x	0	0	0	0	-2.712
μ_y	0	0	0	0	-0.169
μ_z	0	0.29	0	-3.920	0.716
μ^{*2}	0	0.12	0	11.85	1.91
θ_{xx}	0.798	1.085	-3.22	-1.754	-5.375
θ_{yy}	0.798	1.085	-3.22	-1.754	2.250
θ_{zz}	-1.596	-2.170	6.44	3.508	3.125
ϵ	98.723	100.780	167.708	122.996	244.066
$\frac{4}{6\pi}\sigma^3$	9.872	17.875	24.003	13.380	15.248
m	0.948	0.90	0.9563	1.797	2.543
with effective multipole moments:					
μ_x	0	0	0	0	-2.807
μ_y	0	0	0	0	-0.175
μ_z	0	0.266	0	4.030	0.741
μ^{*2}	0	0.10	0	14.51	2.08
θ_{xx}	0.771	0.914	-2.87	-1.837	-5.536
θ_{yy}	0.771	0.914	-2.87	-1.837	2.318
θ_{zz}	-1.542	-1.828	5.74	3.674	3.128
ϵ	98.248	105.255	186.877	103.357	241.265
$\frac{4}{6\pi}\sigma^3$	15.331	17.550	21.733	13.228	15.325
m	0.967	0.90	0.980	1.872	2.516

Table 3: Accuracy of the PC-SAFTP2 model for several systems using ab initio gas phase multipole momentes and efective ones computed using a CSM.

	$\overline{\frac{p_{\mathrm{calc}}-p_{\mathrm{exp}}}{p_{\mathrm{exp}}}}$ in %	$\overline{\frac{v_{\mathrm{l,\ calc}}-v_{\mathrm{l,\ exp}}}{v_{\mathrm{l,\ exp}}}}$ in %	$\overline{\frac{\Delta H_{\mathrm{vap,\ calc}}-\Delta H_{\mathrm{vap,\ exp}}}{\Delta H_{\mathrm{vap,\ exp}}}}$ in %
N_2, QM	0.18	0.44	—
N_2, effective	0.14	0.42	—
CO, QM	3.7	1.1	4.6
CO, effective	1.7	1.0	1.7
C_2H_2, QM	5.3	4.1	—
C_2H_2, effective	2.8	2.0	—
$NCCH_3$, QM	3.1	2.8	4.9
$NCCH_3$, effective	3.6	3.9	4.0
butanone, QM	2.5	2.2	2.5
butanone, effective	2.2	1.9	1.3

10 Figure Captions

Figure 1: SAFT chain with $m = 8$ segments and one dipole. Left: Scheme of the PC-SAFTP1 model where, for the electrostatic interactions, the chain is approximated by a hard sphere of equal molecular volume. Right: The PCP-SAFT approach is based on a 2CLJ fluid with aligned multipole moment for electrostatic interactions stretching over a maximum of two segments.

Figure 2: (Left): 2CLJ particle of elongation L, dipole D and deflection angle γ between dipole axis and the 2CLJ body axis. (Right): The mutual arrangement of two dipolar 2CLJ particles is determined by five angles $\alpha_1, \alpha_2, \omega_1, \omega_2, \phi_{12}$ and the distance r_{12}.

Figure 3: Comparison of simulation data (symbols connected by solid lines) and 2CLJ-P1 and 2CLJ-PCP data for the vapor pressure for 2CLJ fluids with $\mu^{*2} = 6$ and $L^* = 0.6$ for different deflection angles. EOS-based curves go up to the critical point while only the actually computed points are shown for the simulations.

Figure 4: Comparison of simulation data (symbols connected by solid lines) and 2CLJ-P1 and 2CLJ-PCP data for the densities of coexisting phases for 2CLJ fluids with $\mu^{*2} = 6$ and $L^* = 0.6$ for different deflection angles.

Figure 5: Comparison of simulation data (symbols connected by solid lines) and 2CLJ-P1 and 2CLJ-PCP data for the enthalpy of evaporation for 2CLJ

fluids with $\mu^{*2} = 6$ and $L^* = 0.6$ for different deflection angles.

Figure 6: Dipole interaction and spacial hindrance for three mutual particle orientations. The shaded region indicates the interaction strength and the solid straight line the symmetry axis of the 2CLJ body.

Figure 7: Deviation of vapor pressure results of the 2CLJ-P1 model from simulation results based on the original multipole moments and effective ones computed via a CSM.

Figure 8: Deviation of saturated liquid density results of the 2CLJ-P1 model from simulation results based on the original multipole moments and effective ones computed via a CSM.

Figure 9: Comparison of the modified PCP model to molecular simulation data for the vapor pressure of 2CLJ fluids with $L^* = 0.6$ at various dipole-angles.

Figure 10: Comparison of the modified PCP model to molecular simulation data for the vapor pressure of 2CLJ fluids with $L^* = 0.6$ at various dipole-angles.

Figure 11: Effective reduced multipole moments used in the P1 model. The solid lines are obtained by adjusting D^*_{eff} to simulated VLE data, the dashed lines are computed from the dielectric screening energies.

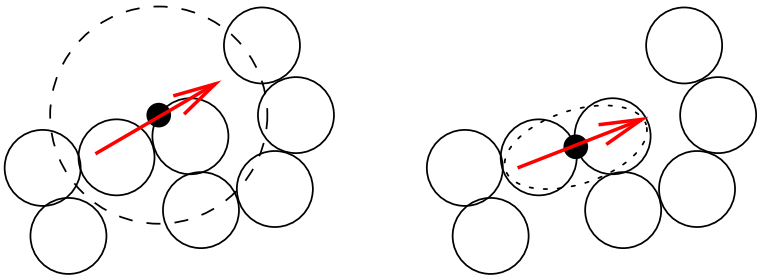

Figure 1:

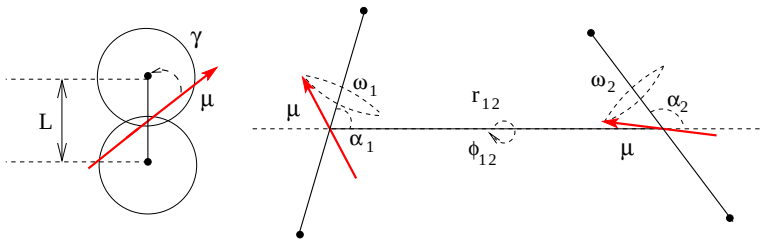

Figure 2:

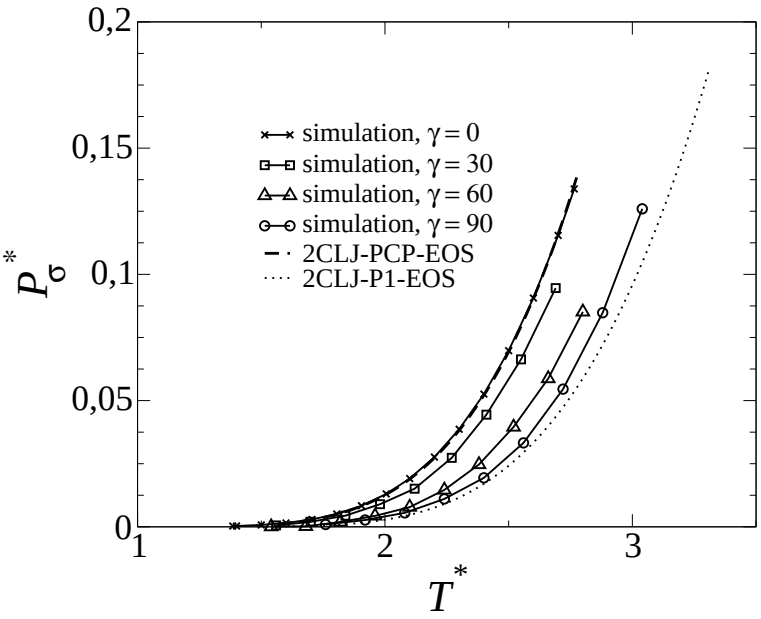
0,2
0,15
0,1
0,05
0
1
2
3
P^*_σ
T^*
simulation, γ = 0
simulation, γ = 30
simulation, γ = 60
simulation, γ = 90
2CLJ-PCP-EOS
2CLJ-P1-EOS

Figure 3:

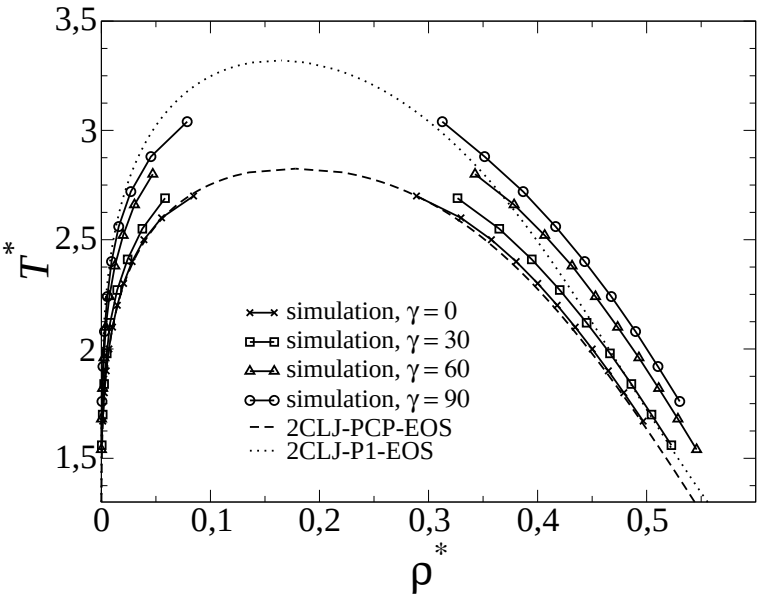
3,5
3
2,5
2
1,5
0
0,1
0,2
0,3
0,4
0,5
T*
ρ*
simulation, γ = 0
simulation, γ = 30
simulation, γ = 60
simulation, γ = 90
2CLJ-PCP-EOS
2CLJ-P1-EOS

Figure 4:

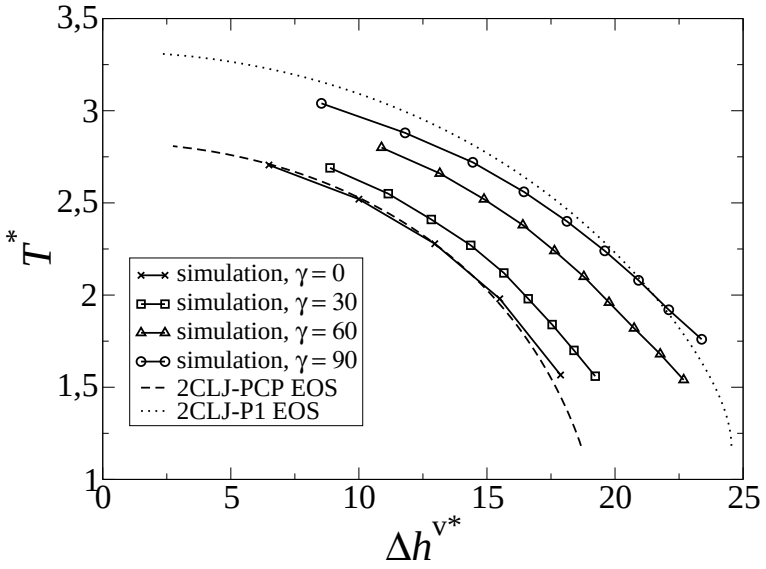
3,5
3
2,5
2
1,5
1
0
5
10
15
20
25
T^*
Δh^{v*}
simulation, γ = 0
simulation, γ = 30
simulation, γ = 60
simulation, γ = 90
2CLJ-PCP EOS
2CLJ-P1 EOS

Figure 5:

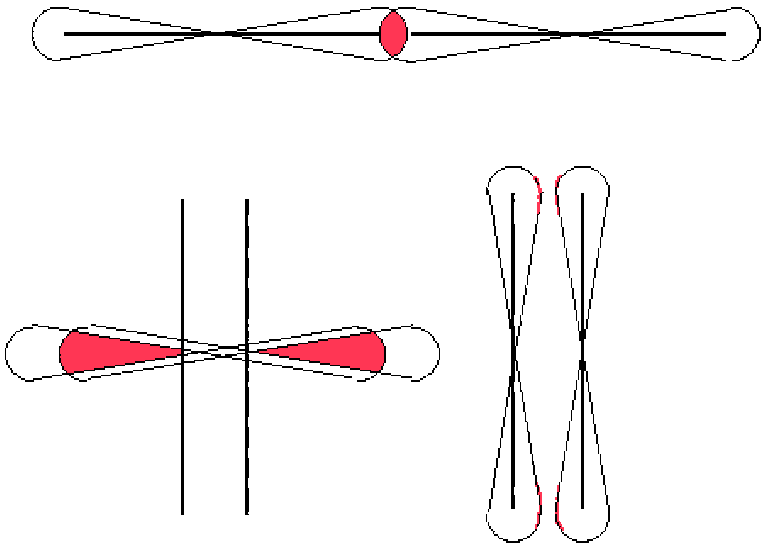

Figure 6:

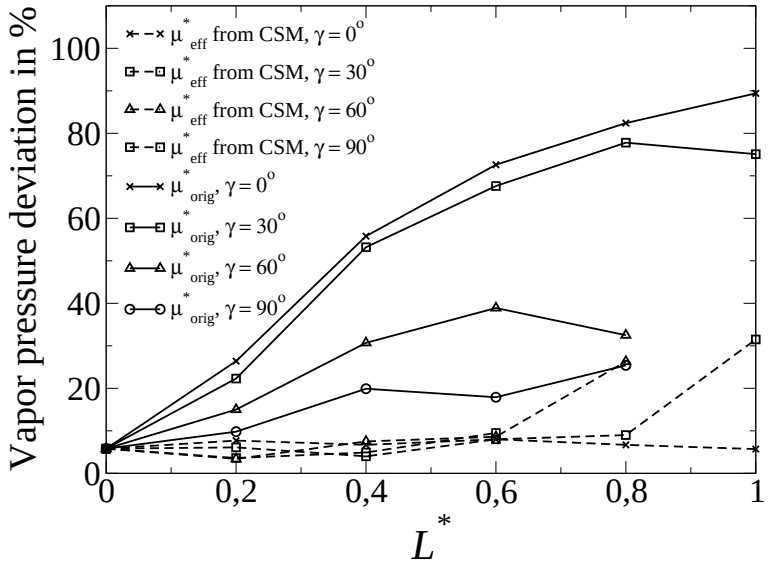
Vapor pressure deviation in %
100
80
60
40
20
0
0
0,2
0,4
0,6
0,8
1
L*
μ*eff from CSM, γ = 0°
μ*eff from CSM, γ = 30°
μ*eff from CSM, γ = 60°
μ*eff from CSM, γ = 90°
μ*orig, γ = 0°
μ*orig, γ = 30°
μ*orig, γ = 60°
μ*orig, γ = 90°

Figure 7:

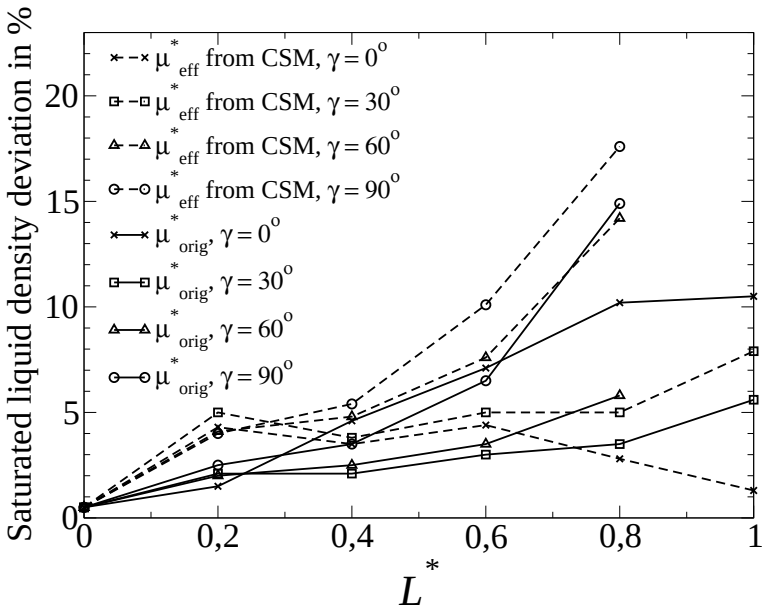
Saturated liquid density deviation in %
L^*
μ^*_{eff} from CSM, $\gamma = 0^o$
μ^*_{eff} from CSM, $\gamma = 30^o$
μ^*_{eff} from CSM, $\gamma = 60^o$
μ^*_{eff} from CSM, $\gamma = 90^o$
μ^*_{orig}, $\gamma = 0^o$
μ^*_{orig}, $\gamma = 30^o$
μ^*_{orig}, $\gamma = 60^o$
μ^*_{orig}, $\gamma = 90^o$
0
5
10
15
20
0
0,2
0,4
0,6
0,8
1

Figure 8:

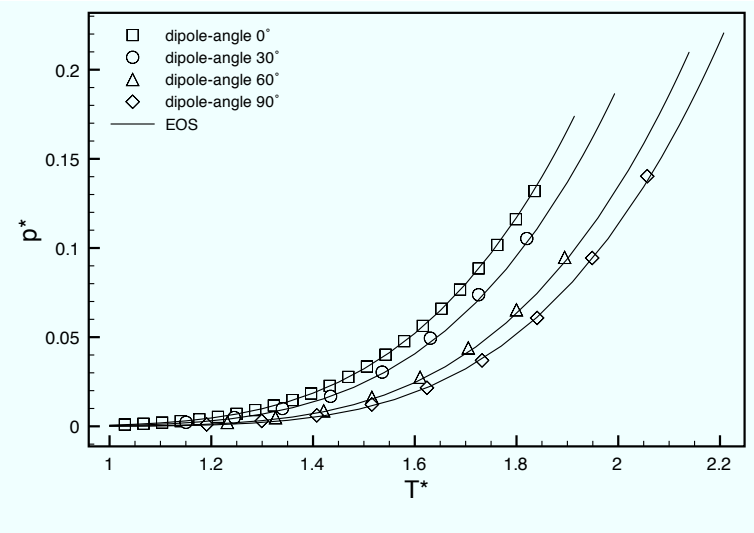
dipole-angle 0˚
dipole-angle 30˚
dipole-angle 60˚
dipole-angle 90˚
EOS
p*
T*
0
0.05
0.1
0.15
0.2
1
1.2
1.4
1.6
1.8
2
2.2

Figure 9:

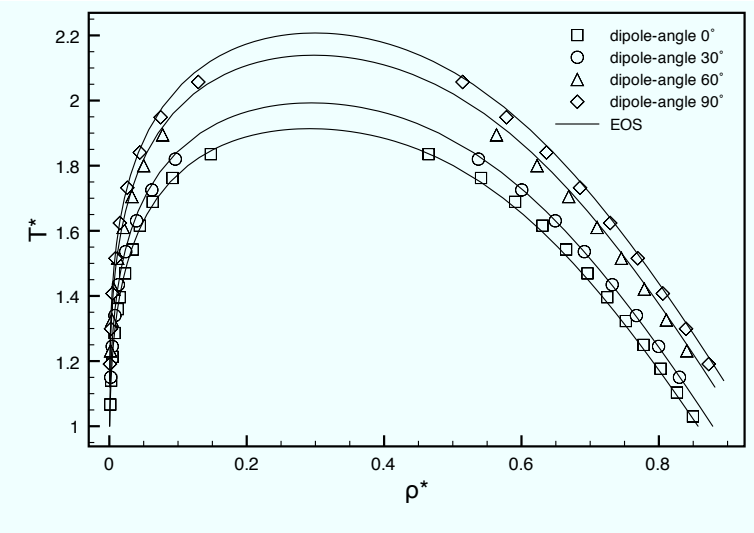
dipole-angle 0°
dipole-angle 30°
dipole-angle 60°
dipole-angle 90°
EOS
T*
ρ*
2.2
2
1.8
1.6
1.4
1.2
1
0
0.2
0.4
0.6
0.8

Figure 10:

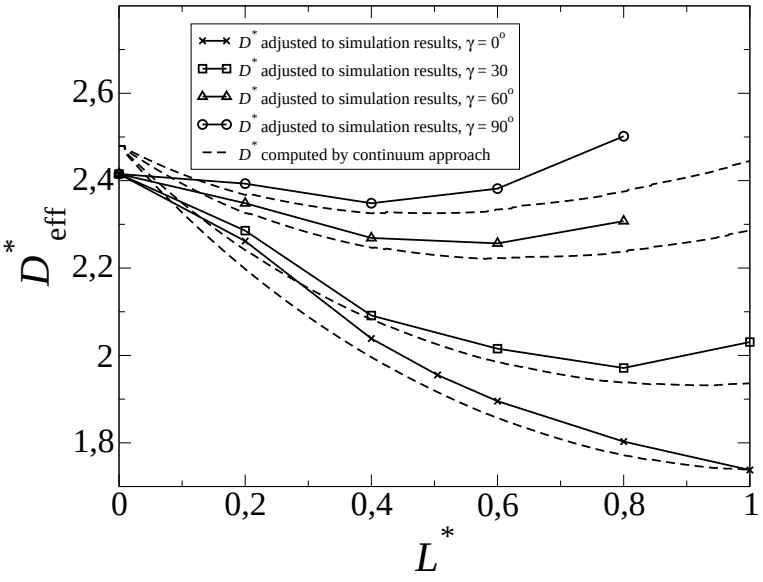
D* adjusted to simulation results, γ = 0°
D* adjusted to simulation results, γ = 30
D* adjusted to simulation results, γ = 60°
D* adjusted to simulation results, γ = 90°
D* computed by continuum approach
2,6
2,4
2,2
2
1,8
0
0,2
0,4
0,6
0,8
1
D* eff
L*

Figure 11: